Passive Transport of C_{60} Fullerenes through a Lipid Membrane: A Molecular Dynamics Simulation Study

Dmitry Bedrov,* Grant D. Smith, Hemali Davande, and Liwei Li

Department of Materials Science & Engineering, 122 South Central Campus Drive Room 304, University of Utah, Salt Lake City, Utah 84112

Received: July 2, 2007; In Final Form: November 18, 2007

To investigate the implications of the unique properties of fullerenes on their interaction with and passive transport into lipid membranes, atomistic molecular dynamics simulations of a C_{60} fullerene in a fully hydrated di-myristoyl-phoshatidylcholine lipid membrane have been carried out. In these simulations the free energy and the diffusivity of the fullerene were obtained as a function of its position within the membrane. These properties were utilized to calculate the permeability of fullerenes through the lipid membrane. Simulations reveal that the free energy decreases as the fullerene passes from the aqueous phase, through the head group layer and into the hydrophobic core of the membrane. This decrease in free energy is not due to hydrophobic interactions but rather to stronger van der Waals (dispersion) interactions between the fullerene and the membrane compared to those between the fullerene and (bulk) water. It was found that there is no free energy barrier for transport of a fullerene from the aqueous phase into the lipid core of the membrane. In combination with strong partitioning of the fullerenes into the lipidic core of the membrane, this "barrierless" penetration results in an astonishingly large permeability of fullerenes through the lipid membrane, greater than observed for any other known penetrant. When the strength of the dispersion interactions between the fullerene and its surroundings is reduced in the simulations, thereby emulating a nanometer sized hydrophobic particle, a large free energy barrier for penetration of the head group layer emerges, indicating that the large permeability of fullerenes through lipid membranes is a result of their unique interaction with their surrounding medium.

I. Introduction

The rate of production of carbon-based nanoparticles (e.g., C_{60} fullerenes and carbon nanotubes), and hence the rate of their introduction into the environment, is increasing rapidly. Additionally, a wide variety of compounds incorporating carbon nanoparticles, particularly fullerenes, for biomedical and drug-delivery applications have either been developed or are under development.[1−6] Studies have revealed that through chemical modification it is possible to control the time for excretion of water-soluble fullerenes from the body. Furthermore, with appropriate modification, fullerene molecules can migrate through the entire body, including the blood−brain barrier, without adsorbing serum proteins.[7−9] Examples of biomedical applications of fullerene molecules include DNA-modified fullerenes that target double-stranded DNA and cleave it,[10] HIV protease inhibitors,[11] skin cancer treatments,[7] vectors for transfection with potential application in gene therapy of diseases,[12] antioxidant drugs for neurodegenerative diseases,[3,13−16] and efficient contrast agents for magnetic resonance imaging.[17]

Whenever any synthetic material is introduced into a biological system, either through design or through environmental uptake, issues of biocompatibility and potential deleterious health effects are of paramount importance. A few studies of the interaction of carbon nanoparticles with proteins and nucleotides have been reported.[18,19] While there is still controversy as to whether pristine C_{60} and its derivatives are health and environmentally dangerous[20] there is strong evidence that fullerenes can be cytotoxic[21−23] and that the exposure of living cells to C_{60} fullerene derivatives and that their aggregates can result in disruption of the cell membrane due to lipid peroxidation.[24] An improved fundamental understanding of interactions between fullerenes and cell membranes is central to understanding potential deleterious effects of fullerenes and fullerene-based molecules on living cells as well as to help in the design of effective nanoparticle-based biomaterials. Recently, we have shown through molecular dynamics (MD) simulation studies that because of their size (approximately 1 nm in diameter) and strong van der Waals (dispersion) interactions (due to a high density of surface atoms), fullerenes behave neither like classical hydrophobic molecules nor like hydrophobic surfaces.[25−27] We found that association of a pair of C_{60} fullerenes is dominated by the strong direct fullerene−fullerene attractive interactions. Surprisingly, water-induced interactions between the fullerenes were found to be repulsive. Specifically, it was found that the high atomic density on the fullerene surface gives rise to highly favorable water−fullerene interactions due to strong carbon−water dispersion interactions. The energetic origin of this water-induced repulsive interaction between the carbon nanoparticles is in stark contrast to the entropy-driven association observed for conventional hydrophobic nonpolar organic solutes.

To investigate the implications of the unique properties of fullerenes on their interaction with and passive transport into lipid membranes, we have conducted all-atom MD simulations of a C_{60} fullerene in a fully hydrated di-myristoyl-phoshatidylcholine (DMPC) lipid membrane. To date computational studies of molecule transport in lipid membranes have been primarily

* To whom correspondence should be addressed. E-mail: bedrov@cluster2.mse.utah.edu.

10.1021/jp075149c CCC: $40.75
Published on Web 01/30/2008

limited to small molecules.[28−44] A few atomistic simulations studies[45,46] have looked at the interaction of carbon-based nanoparticles with model cell membranes but have not addressed the permeability of these nanoparticles through cell membrane. Only two simulation works address issues of permeability of fullerenes through model cell membranes. The first employed a coarse-grained model to investigate the transport of model nanoparticles (fullerene-like) through a model lipid membrane.[47] While this work showed some qualitative consistency with atomistic simulations discussed below the results of these simulations should be taken with caution due to relatively crude representation of water and lipid molecules. The second study utilized atomistic simulations to compare transport of C_{60} and $C_{60}(OH)_{20}$ from water into a di-palmitoyl-phosphatidylcholine (DPPC) bilayer[48] and found that a pristine fullerene can readily "jump" into the bilayer and translocate through membrane, while $C_{60}(OH)_{20}$ was not able to do so over the entire length of the simulation. The authors explained the observed difference in the ability of the pristine and OH-modified fullerenes to penentrate into the bilayer by analyzing the potential of mean force (PMF) acting on the fullerene as a function of its position relative to the bilayer center of mass. However, as we discuss below, the PMF obtained from that work is inconsistent with our data as well as experimental data on solubility of fullerenes in different environments.

II. Computational Methods

A. Force Field. The bilayer studied in our simulations is shown in Figure 1 and consists of 52 DMPC molecules and 1800 water molecules. The force field parameters for lipid molecules were taken from CHARMM27.[49] The intra- and intermolecular potentials for water were taken from the TIP3P model.[50] The carbon−carbon interaction in C_{60} was described by a Lennard-Jones potential with $\sigma_{CC} = 3.47$ Å and $\epsilon_{CC} = 0.275$kJ mol^{-1} as utilized in previous simulations of C_{60}.[51] For the interactions between C_{60} and water, a Lennard-Jones potential with $\sigma_{CO} = 3.19$ Å and $\epsilon_{CO} = 0.392$ kJ mol^{-1} was utilized.[25] Nonbonded interactions are included between all atoms of different molecules and between atoms of the same molecule separated by more than two bonds. Geometric combining rules were utilized to calculate interactions between C_{60} and DMPC as well as water and DMPC. We have previously employed this potential in simulations of C_{60} fullerenes in aqueous environments.[25−27,52]

B. Simulation Protocol. Simulations were carried out using the MD simulation package *Lucretius* (http://lucretius.mse.utah.edu). The Nose−Hoover thermostat[53,54] was used to maintain the temperature at 310 K. The Anderson−Hoover barostat[54,55] was used for pressure control and was adapted to accommodate the periodic orthorhombic simulation cell. All bonds of fullerenes, water, and bonds of DMPC involving hydrogen atoms were constrained utilizing the SHAKE algorithm.[56] A cutoff radius of 12.5 Å was used for all van der Waals interactions. The long-range truncation corrections due to van der Walls interactions have been applied for pressure, forces, and potential energy. For directions parallel to the bilayer (x and y) the long-range truncation corrections have been calculated using conventional formulations[57] that assume that for separations larger than cutoff radius the pair correlation function $g(r) \approx 1$. However, this assumption is not valid in the normal direction (z) of lipid bilayer due to structure anisotropy in this direction. Therefore, the long-range truncation corrections in the z direction were calculated using density profiles for each type of nonbonded interaction that were regularly updated during simulation. To account for long-range electrostatic interactions, the Particle Mesh Ewald algorithm[58] was used. A multiple time step reversible reference system propagator algorithm[59] was employed for integrating equations of motion. A time step of 0.2 fs was used for integration of vibrational degrees of freedom (bonds, bends, and torsions). Nonbonded interactions within a cutoff radius of 6 Å were evaluated every 2.5 fs, while those between 6 and 12.5 Å as well as reciprocal part of electrostatic calculations were evaluated every 5 fs.

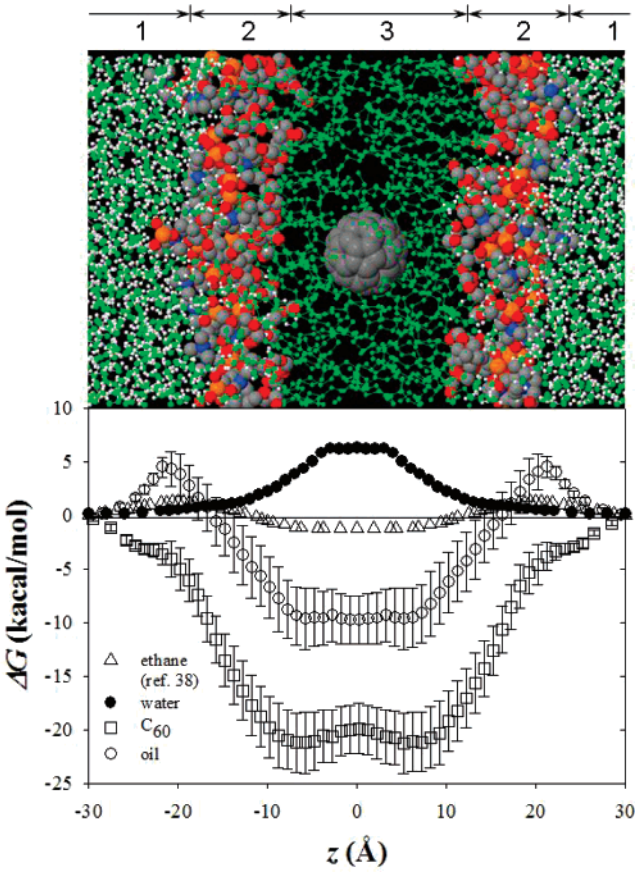

Figure 1. Relative free energy as function of penetrant position relative to the center-of-mass of lipid membrane obtained from our MD simulations for water, C_{60} fullerene, and oil nanodroplet as well as for ethane from ref 38. Top panel shows system configuration with a snapshot of the hydrated DMPC membrane containing a C_{60} fullerene and illustrates three well-defined regions: (1) bulk water outside of lipid bilayer, (2) dense layer of lipid hydrophilic head groups, and (3) hydrophobic region of lipidic tails. Hydrogen atoms associated with lipid tail are not shown. Fullerene carbon atoms are shown in dark gray, water oxygen atoms in green, and hydrogen atoms in white. In the DMPC molecule: tail backbone carbon atoms are dark lime, nitrogens dark blue, phosphorus atoms orange, and oxygen atoms red.

The model membrane system was equilibrated using an NP_NAT (constant number of particles, normal pressure, cross-sectional area, and temperature = 310 K) ensemble for about 3 ns. The simulations were run with a fixed lipid surface area of 61.8 Å^2 per DMPC molecule. The normal direction was subjected to isothermal−isobaric constraints to maintain an equilibrium normal stress (1 atm), yielding a mean size of 69.07 Å in the z direction. Janiak et al. have reported the area per head group for model DMPC membrane to be 62 Å^2 from their X-ray diffraction studies at 308 K.[60] Production runs for calculation of constraint force (see below) at each separation were carried out in an NVT ensemble over 8 ns using a 40.11 × 40.11 × 69.07 Å^3 orthorhombic cell.

C. Property Calculations. To determine the free energy profile $\Delta G(z)$ for penetration of C_{60} and water through the

DMPC membrane, the center-of-mass of the solute molecule (C_{60} or water) was constrained along the bilayer normal (z axis) at various separations from the center of mass of the bilayer. For C_{60}, simulations at 60 separations with increments of 0.5 Å for $0.0 < z < 26.0$ Å and 1.0 Å for $26.0 < z < 34.0$ Å were conducted to obtain an accurate constraint force and free energy profile. For water, simulations at 28 separations with increments of 1.0 Å for $0.0 < z < 22.0$ Å and 2.0 Å for $22.0 < z < 34.0$ Å were conducted. Each solute was completely free to move in the xy plane. The constraint force between the center-of-mass of the fullerene (water) molecule and the bilayer was recorded every 10 fs, while the average (over the entire trajectory) force was integrated to obtain the free energy profile as a function of solute position relative to the bilayer center-of mass. Because production runs were conducted in the *NVT* ensemble we have confirmed that constraining of fullerene position relatively to the bilayer center-of-mass does not result in an increase of lateral pressure as the fullerene penetrates through relatively dense layer of lipid head groups. Lateral dimensions of our simulations were large enough to show no dependence (within statistical uncertainty) of the lateral components of the stress tensor on position of the fullerene in the system.

Following Berendsen and Marrink,[33,34] we have calculated position-dependent diffusion coefficient $D(z)$ of the permeating solute (water and C_{60}). This calculation is based on a condition that local time dependent friction coefficient $\xi(t)$ of a solute is related to the time autocorrelation function of the fluctuations in the force acting on the solute molecule $F(z,t)$ from the average $\langle F(z)\rangle$. This condition is met when the diffusive motion of the solute on the time scale of the relaxation of the force correlation function results in a change of the solute chemical potential (due to a free energy gradient) that is less than or comparable to thermal fluctuations, i.e., k_BT). For each position of the solute $D(z)$ can be obtained as[33,34]

$$D(z) = \frac{RT}{\xi} = \frac{(RT)^2}{\int_0^\infty \langle \Delta F(z,t)\Delta F(z,0)\rangle dt} \quad (1)$$

where $\xi = \int_0^\infty \xi(t)dt$ is the static friction coefficient and $\Delta F(z,t)$ denotes the deviation of the instantaneous force acting on the solute molecule constrained at position z from the average force. Subsequently, the permeability of the solute P can be found from the local resistance to permeation, $\mathcal{R}(z')$, at depth z' using[33,34]

$$\frac{1}{P} = \int_{\text{outside}}^{z} \mathcal{R}(z')\, dz' = \int_{\text{outside}}^{z} \frac{\exp(\Delta G(z')/RT)}{D(z')}\, dz' \quad (2)$$

D. Uncertainty Estimation. It is important to make sure that the sampling of the constraint force has converged during simulation for each separation of the solute and the bilayer. For small solutes such as water, sampling over a few hundred picoseconds is sufficient.[34] However, for the larger C_{60} fullerene the trajectory length needs to be much longer. In Figure 2 we show the running average of the constraint force as a function of total trajectory length for several selected fullerene−bilayer separations for which simulations have been extended to 15 ns total. We found that after about 4 ns of sampling the average force for most separations saturates near the long time average value. This indicates that a trajectory length over at least 4 ns is necessary to obtain a reasonable estimate for the average constraint force on the C_{60} fullerene.

To estimate uncertainties for calculated free energy profiles we have divided the total trajectory into four equal subsets and have calculated the average constraint force for each subset. Using the subset average values the free energy profiles have been calculated for each subset as described above. Then a standard error analysis (68% confidence level) using four data points for free energy at each separation have been conducted.

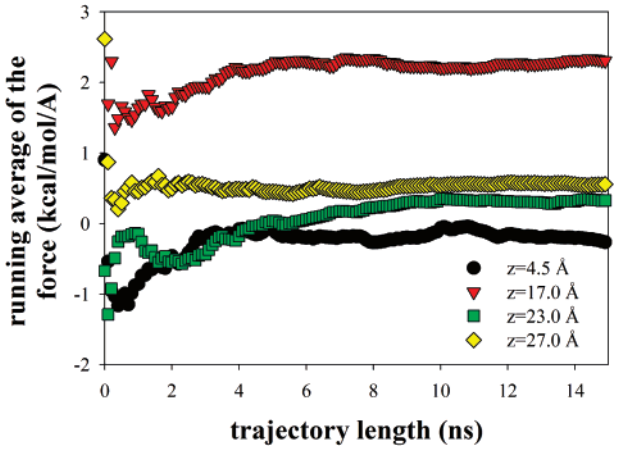

Figure 2. Running average of the constrain force shown as a function of trajectory length for several separations.

III. Results

A. Free Energy Profile. Figure 1a shows a snapshot of a C_{60} fullerene in a fully hydrated DMPC lipid membrane obtained from our simulations. The fullerene is sitting near the center-of-mass plane of the membrane, denoted as $z = 0$. In Figure 1b the free energy of the fullerene−membrane system as a function of the position of the fullerene is shown. The free energy, ΔG, has been calculated relative to that when the fullerene is in the bulk water phase ($|z| > 30$ Å) and well separated from the membrane. Also shown are free energy difference for a water molecule (this work) and an ethane molecule.[38] The free energy profile for water is in good agreement with that obtained from previous simulations[38] and exhibits behavior typical of small hydrophilic molecules in lipid membranes, namely, limited solubility in the lipidic core of the membrane that results in a monotonic increase in free energy as the water penetrates from the water phase into the membrane. In contrast, the free energy profile for ethane rises relatively steeply as the hydrophobic molecule penetrates the tightly packed, highly polar head group region of the membrane and then decreases rapidly within the lipidic core. The lower free energy of ethane within the lipid core compared to the water phase indicates a strong partitioning of the hydrophobic molecule into the membrane.

Figure 1b reveals that the free energy of C_{60} in water is higher by 20 (±2) kcal/mol than in the lipidic core of the membrane, indicating a strong partitioning of the fullerenes into the membrane as is seen for small hydrophobic penentrants (e.g., ethane). In our previous work,[61] we demonstrated that the environment for a C_{60} fullerne at the center of the lipid membrane is similar to that experienced in an alkane melt. The favorable free energy associated with C_{60} in the core of the membrane compared to C_{60} in the water phase is consistent with the relative solubility of C_{60} in alkanes compared to water. Trace analysis of C_{60} in water, obtained from a highly sensitive transient absorption spectrometry, has indicated that the solubility of C_{60} in water is less than 0.1 ng/L,[62] while ref 2 reports solubility of about 1×10^{-12} ng/L. On the other hand, the solubility of C_{60} at 303 K in decane is 70 mg/L,[63,64] in dodecane is 91 mg/L, and in tetradecane is 126 mg/L.[63] Assuming that ΔG for moving fullerene from water inside the middle of the

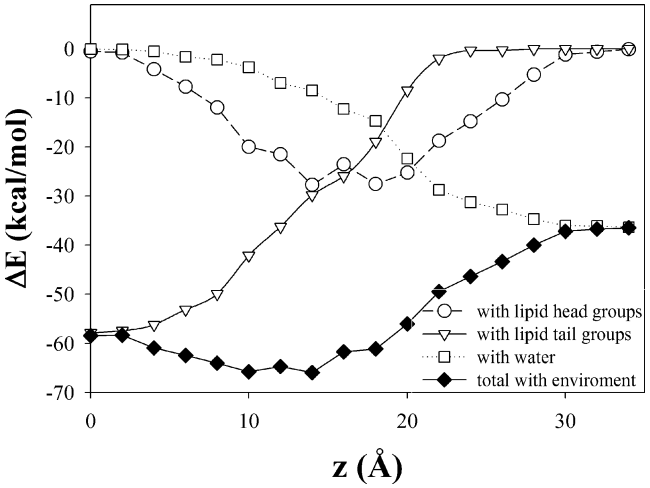

Figure 3. Nonbonded energy of C_{60} interaction with environment as a function of fullerene position. Also shown are the contributions from C_{60} interactions with water, lipid tails, and lipid heads.

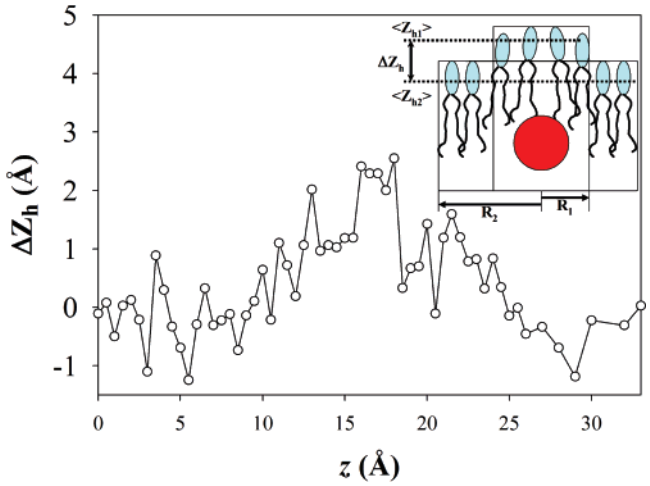

Figure 4. Difference in average position (in the z direction) of lipid head groups close to fullerene (within the cylinder of $R_1 = 7$ Å) and head groups of neighboring lipids (those which are outside of cylinder R_1 but inside of larger cylinder $R_2 = 11$ Å) as schematically illustrated on the inset.

bilayer can be estimated using experimental solubilities $\Delta G = k_B T \ln(S_{water}/S_{alkane})$ then one should expect ΔG to be somewhere between −12 kcal/mol (assuming $S_{water} = 0.1$ ng/L) and −45 kcal/mol (assuming $S_{water} = 1 \times 10^{-12}$ ng/L). Calculations using the polarizable continuum model[65] predicted −24 kcal/mol free energy difference between solvation of C_{60} fullerene in water and in *n*-hexane. The $\Delta G = -20$ kcal/mol obtained from our simulations is consistent with these numbers. However, simulations reported in ref 48 predict the ΔG for fullerene translocation from water into the middle of the bilayer (where the environment is very similar to alkane melt[61]) on the order of −3 kcal/mol, which is significantly less than predictions from our simulations as well as inconsistent with experimental solubility data.

Unlike small hydrophobic molecules, we have shown in recent simulations[61] that the relative favorability of alkane-C_{60} fullerene interactions compared to water−fullerene interactions is due to the stronger dispersion interactions between alkanes and fullerenes compared to water and fullerenes and not due to any inherent hydrophobicity of the fullerenes. This is clearly illustrated in Figure 3 where the energy due to interaction of C_{60} fullerene with its environment is shown as a function of fullerene position. Also shown are the contributions to this energy from interaction of C_{60} with water, lipid tails, and lipid heads. Figure 3 indicates that by taking a fullerene from bulk water ($z > 30$ Å) and placing it in the middle of the bilayer ($z = 0.0$ Å) fullerene interaction with the environment becomes more favorable by about 22 kcal/mol. Examination of different contributions to the C_{60} fullerene interactions shows that this energy difference is comprised of about 58 kcal/mol reduction due to interactions with lipid tails and 36 kcal/mol gain due to loss of interaction with water. These contributions clearly illustrate that the lipid tails provide a more favorable environment for C_{60} dispersion interactions than bulk water.

Comparison of free energy (Figure 1b) and total C_{60}−enviroment interaction energy (Figure 3) shows that, while C_{60} has the most favorable interaction (Lennard-Jones energy) with its surroundings at a position of 10−15 Å from the bilayer center, the minimum in the free energy is around a position of 6−7 Å. Moreover, the free energy steeply increases as the C_{60} fullerene moves more than 8 Å from the center of the bilayer despite the favorable nonbonded interaction with surrounding. This mismatch in position of the minima for the energy and the free energy can be explained by distortion of the bilayer.[61]

For positions larger than 8 Å away from the center of the bilayer the fullerene begins to penetrate into the more structured head group region causing significant structural distortion illustrated in Figure 4 where the relative position of head groups for lipids which are located near the fullerene is compared to the position of head groups of neighboring lipids. Specifically, we have defined a cylinder of radius $R_1 = 7$ Å, which is normal to the lipid bilayer and with an axis going through the fullerene center-of-mass as schematically shown on the inset of Figure 4. Then, the average of head group positions (defined by phosphorus atoms), which are inside the cylinder and are located in the same half of the lipid bilayer (upper or lower) as the fullerene, were calculated ($\langle Z_{h1} \rangle$). This average position was compared with the average position of head groups of neighboring lipids ($\langle Z_{h2} \rangle$), which are located inside of a larger cylinder $R_2 = 11$ Å but outside of the smaller cylinder. $\Delta Z_h = \langle Z_{h1} \rangle - \langle Z_{h2} \rangle$ as a function of fullerene position in the lipid bilayer is shown in the main panel of Figure 4. It can be clearly seen that penetration of the fullerene inside the bilayer tails by more than 8 Å away from the bilayer center-of-mass results in displacement of nearby head groups by as much as 2 Å relative to other lipids. This displacement can noticeably disrupt the lipid−lipid interactions and hence be energetically unfavorable. Therefore, the observed preferred position (minimum in free energy) for the fullerene shown in Figure 1a reflects not only fullerene−bilayer interaction energy but also additional factors such as distortion of the DMPC structure and disturbance of hydrogen-bonding in the DMPC head group region.

A C_{60} fullerene in the DMPC membrane behaves like neither a small hydrophilic nor a small hydrophobic molecule. In contrast to a small hydrophobic penetrant (ethane), penetration of the C_{60} fullerene through the highly polar head group region of the membrane is not associated with a free energy barrier, as shown in Figure 1b. The free energy is actually lower when the fullerene is in the tightly packed, highly polar head group region than in the bulk water phase. Hence, consistent with our previous simulation studies of fullerenes in water,[25−27] the free energy profile for fullerenes indicates that the nonpolar fullerene does not exhibit an intrinsic aversion to highly polar environments. This is due to the strong van der Waals interactions between C_{60} fullerenes and their environment that is a consequence of the high atomic density on the fullerene surface. Compared to an equivalently sized (1 nm diameter) oil droplet,

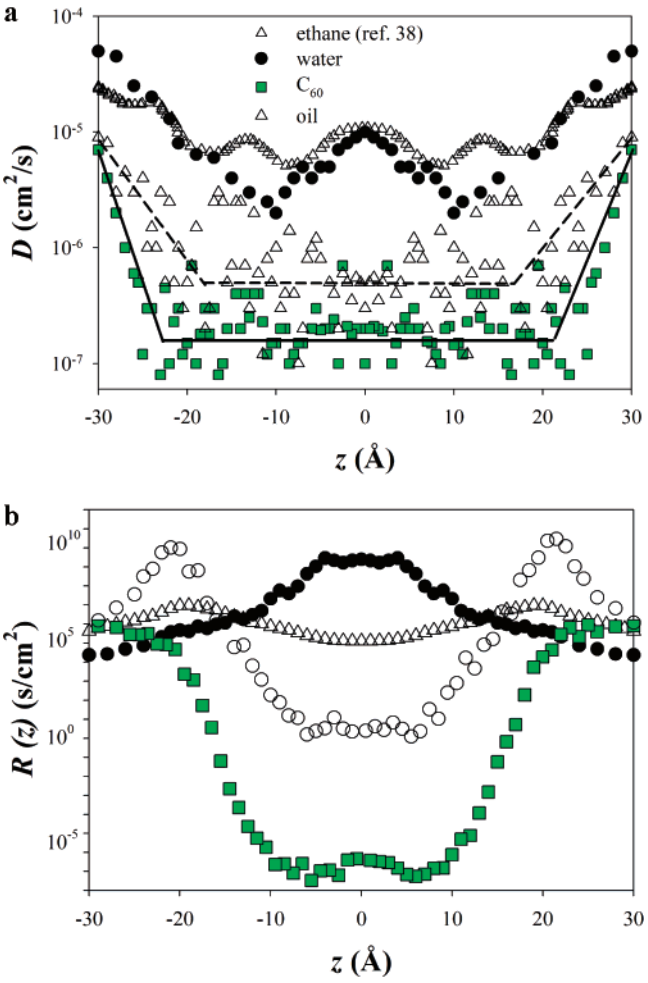

Figure 5. Local diffusion coefficient (for motion along the bilayer normal) (a) and resistance to permeation (b) of C_{60} fullerene, oil nanodroplet, water, and ethane as a function of position relative to the bilayer center-of-mass. Lines are for eye guidance.

fullerene surfaces have almost four times as many carbon atoms per unit area,[25] and as a result both polar and nonpolar molecules interact preferentially with fullerenes like molecules. Because the membrane is denser (from the point of view of dispersion interactions) than water, the fullerene prefers to sit anywhere within the membrane than in bulk water, with the most favorable interactions occurring near the center of the bilayer.

A remarkably consequence of the van der Waals dominated interactions of the C_{60} fullerene with its environment is the "barrierless" penetration of the membrane illustrated in Figure 1b. The absence of the free energy barrier implies that the fullerene placed in the water phase should have no problem of penetrating inside the membrane over the course of the simulation. We have conducted additional simulations where the fullerene was originally placed in the water phase near the bilayer and then was allowed to freely move (no constrain) during the simulation. After 8 ns of simulation time the fullerene have penetrated inside the lipid bilayer where it remained through the entire simulation. The same phenomenon has been observed in the unbiased simulations of fullerene in ref 48.

B. Diffusion Coefficients and Permeation. The position-dependent diffusion coefficient $D(z)$ (eq 1) for water (this work), C_{60} fullerene (this work), and ethane[38] within the DMPC membrane are shown in Figure 5a. In the water phase the diffusion coefficient of C_{60} is significantly smaller than for water and ethane due to the relatively large size of the fullerene. Within the membrane the diffusion coefficient of water decreases with penetration following the density profile of water within the membrane (not shown). Near the center of the membrane the diffusion coefficient of water increases, perhaps due to reduced density and increased mobility of the lipid tails. Our position-dependent diffusion coefficient for water is in good agreement with that reported previously.[38] The diffusion coefficient for the representative small hydrophobic molecule (ethane) is reduced within the membrane compared to that in the water phase but shows relatively little dependence on position within the membrane. Qualitatively similar behavior is observed for C_{60} fullerene. Within the lipidic core of the membrane the diffusion coefficient of the fullerene is about 2 orders of magnitude smaller than in the water phase, consistent with our simulations of C_{60} fullerenes in a tridecane melt[61] and appears to show relatively little dependence on relative position of the fullerene inside the membrane.

Equation 1 has been derived under the assumption that the free energy is constant over the correlation distance of the particle.[34] It has been shown that for small penetrates in lipid bilayers that this condition is well satisfied.[34] To confirm the validity of this equation for the C_{60} fullerene we have estimated the maximum change in the free energy that C_{60} fullerene can experience over the correlation distance. The largest gradient in the free energy profile for C_{60} is observed at the boundary between regions 2 and 3 (see Figure 1a) at z around 16.0 Å and is about 2.0 kcal/mol/Å. At this separation, the correlation time for the relaxation of constrain force autocorrelation function is around 30 ps. Using $D(z)$ at this separation, we estimate that correlation distance for the fullerene will be around 0.2 Å. Across this distance the change in free energy is about 0.4 kcal/mol, which is less than thermal fluctuations k_BT, and therefore Brownian diffusion of the fullerene can be expected in this case.[38]

The position dependent resistance to permeation $R(z)$ (eq 2) is shown in Figure 5b for water, ethane, and C_{60}. Resistance in the water phase is greater for the fullerene than for water or ethane due to the smaller diffusion coefficient for the larger fullerene. As the membrane is penetrated, resistance increases monotonically for water primarily due to increasing free energy (or conversely, reduced solubility) as the environment becomes more hydrophobic. Hence, the low solubility of water in the lipidic core of the membrane results in a substantial barrier to water penetration. For the model small hydrophobic molecule resistance is greatest in the tightly packed, highly polar head group region. However, ethane is sufficiently small that the barrier to penetration through the head groups is not large. Since the hydrophobic ethane is highly soluble in the lipidic core, this region does not pose a significant barrier to penetration of the small hydrophobic molecule. Consequently, the permeability of the hydrophobic ethane is greater than that for water, as shown in Figure 6. In general, for molecules sufficiently small such that they do not significantly perturb the head group region, the more hydrophobic the molecule the greater the permeability. As hydrophobic molecules become larger, the barrier for penetration of the head group layer increases substantially and permeability drops dramatically.[66]

On the basis of upon these observations, we might anticipate that the large C_{60} fullerene would have quite low permeability through the lipid bilayer due to significant distortion of the head group layer and hence a large barrier for penetration through the head group layer. To show that if C_{60} were truly hydrophobic that this would indeed be the case, we have conducted additional simulations for permeation of an "oil" droplet with the size equal to C_{60} fullerene. In these simulations, we used the C_{60} geometry

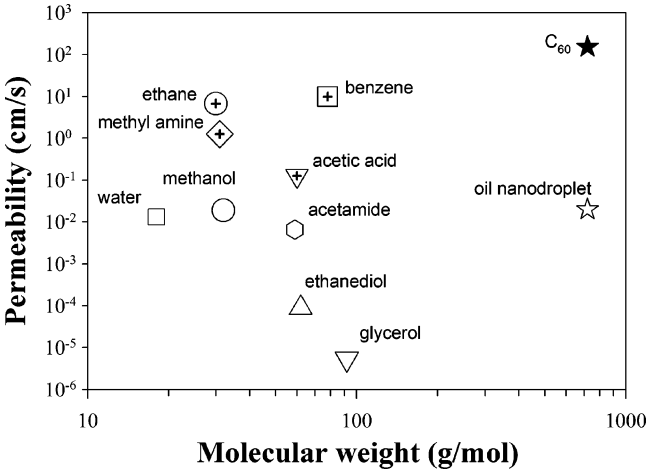

Figure 6. Permeability of various molecules through lipid membranes as a function of penetrant molecular weight. C_{60} and oil nanodroplet data are from this work; all other are simulation data on permeation through DPPC bilayer at 323 K taken from ref 38.

to represent the droplet; however the strength of van der Waals interactions between oil-droplet carbons and environment have been reduced by a factor of 4. We have shown previously that this scaling is a good representation of an oil (tridecane) droplet of 1 nm size using C_{60} molecular geometry.[25] By use of the same simulation protocol and analysis as for pristine C_{60} fullerene, we have calculated constrain force, free energy, and local diffusion coefficient for an "oil" droplet as a function of its position in the system.

The free energy profile for the hydrophobic "oil" droplet is shown in Figure 1b, clearly demonstrating the substantial free energy barrier (about 5 kcal/mol) to penetration of the head group region, in stark contrast to the fullerene. While the head group region is perturbed by both the fullerene and hydrophobic nanoparticle, the strong dispersion interactions between the very dense head group region and the fullerene offsets this effect for the case of a penetrating fullerene. The free energy difference for bringing an oil droplet from water inside the lipid bilayer is about −10 kcal/mol, which is consistent with a hydrophobic nature of this solute. The local diffusion coefficient determined for the "oil" droplet is shown in Figure 5a and is systematically higher than what we obtained for C_{60} fullerene. Figure 5b shows the position dependent resistance for the hydrophobic nanoparticle, and as anticipated, resistance to penetration posed by the head group regime is substantial, resulting in a low permeability as shown in Figure 6.

IV. Discussion

Examination of Figure 6, which shows the calculated (eq 2) permeability of various molecules through lipid membranes, reveals that the permeability of C_{60} fullerenes is significantly greater than that of all other molecules studied. This is due to the unique interactions of the fullerene with its surroundings, specifically strong dispersion interactions. Since the fullerene is neither hydrophilic nor hydrophobic, it behaves like neither type of molecule. Hence, permeability of fullerenes through the lipid membrane is not limited by the head group layer as for large hydrophobic particles due to strong attractive interactions of the fullerene with the dense head group region. Similarly, permeability of the fullerene is not limited by solubility in the lipid core as is found for hydrophilic molecules because of a strong preference for the atomically denser (from the point of view of dispersion interactions) alkane environment compared to the bulk water phase. In fact, the primary limiting factor for permeability of the fullerene through the lipid bilayer is the relatively small diffusion coefficient (Figure 5a) for this large molecule.

As mentioned above, studies have shown that with appropriate modification fullerene molecules can migrate through the whole body without adsorbing serum proteins, including penetration of the blood−brain barrier.[7−9] The latter is particularly striking because the blood−brain barrier blocks almost all substances except those allowed by means of cell membrane solubility or by specific transport systems. Hence most substances with a molecular weight larger than 500 Daltons cannot penetrate through the blood−brain barrier. Since there is no evidence that there are specific transport mechanisms promoting transport of C_{60} fullerenes through cell membranes, it is likely that this relatively large molecule (720 Daltons) penetrates cell membranes by means of passive transport through membrane walls. The high permeability of C_{60} fullerenes through a model lipid membrane predicted from our simulations strongly supports this mechanism. Taking into account that aggregation of fullerenes in aqueous solutions (driven by their strong direct van der Waals interaction) can be prevented by relatively minor chemical modifications[8,11,13] that likely would not strongly affect the interaction of C_{60} with the cell membrane, our simulations also support the proposition that C_{60} fullerenes can serve as efficient carriers that can assist in drug delivery inside and through cell membranes.

Acknowledgment. Authors would like to acknowledge support from the University of Colorado Ferroelectric Liquid Crystal MRSEC funded by the National Science Foundation through Grant DMR0213918.

References and Notes

(1) Dresselhaus, M. S.; Dresselhaus, G.; Eklund, P. C. *Science of fullerenes and carbon nanotubes*; Academic: San Diego, 1996.

(2) Nakamura, E.; Isobe, H. *Acc. Chem. Res.* **2003**, *36*, 807−814.

(3) Osawa, E. Ed. *Perspectives of fullerene nanotechnology*; Kluwer Academic Publishers: Dordrecht, 2002.

(4) Murthy, C. N.; Geckeler, K. E. *Chem. Commun.* **2001**, 1194−1195.

(5) Wilson, L. J.; Cagle, D. W.; Thrash, T. P.; Kennel, S. J.; Mirzadeh, S.; Alford, J. M.; Ehrhardt, G. J. *Coord. Chem. Rev.* **1999**, *190*, 199−207.

(6) Tagmatarchis, N.; Shinohara, H. *Mini Rev. Med. Chem.* **2001**, *1*, 339−348.

(7) Cagle, D. W.; Kennel, S. J.; Mirzadeh, S.; Alford, J. M.; Wilson, L. J. *Proc. Natl. Acad. Sci. U.S.A.* **1999**, *96*, 5282−5187.

(8) Rajagopalan, P.; Wudl, F.; Schinazi, R. F.; Boudinot, F. D. *Antimicrob. Agents Chemother.* **1996**, *40*, 2262−2265.

(9) Tabata, Y.; Murakami, Y.; Ikada, Y. *Jpn. J. Cancer Res.* **1997**, *88*, 1108−1116.

(10) Boutorine, A. S.; Tokuyama, H.; Takasugi,M.; Isobe, H.; Nakamura, E.; Helene, C. *Angew. Chem., Int. Ed. Engl.* **1994**, *33*, 2462−2465.

(11) Marcorin, G. L.; Ros, T. D.; Castellano,S.; Stefancich, G.; Bonin, I.; Miertus, S.; Prato, M. *Org. Lett.* **2000**, *2*, 3955−3958.

(12) Nakamura, E.; Isobe, H.; Tomita, N.; Sawamura, M.; Jinno, S.; Okayama, H. *Angew. Chem., Int. Ed.* **2000**, *39*, 4254−4257.

(13) Wang, I. C.; Tai, L. A.; Lee, D. D.; Kanakamma, P. P.; Shen, C. K. F.; Luh, T.−Y.; Cheng, C. H.; Hwang, K. C.; *J. Med. Chem.* **1999**, *42*, 4614−4620.

(14) Straface, E.; Natalini, B.; Monti, D.; Franceschi, C.; Schettini, G.; Bisaglia, M.; Fumelli, C.; Pincelli, C.; Pellicciari, R.; Malorni, W. *FEBS Lett.* **1999**, *454*, 335−340.

(15) Lin, A. M.; Chyi, B. Y.; Wang, S. D.; Yu, H. H.; Kanakamma, P. P.; Luh, T. Y.; Chou, C. K.; Ho, L. T. *J. Neurochem.* **1999**, *72*, 1634−1640.

(16) Dugan, L. L.; Turetsky, D. M.; Du, C.; Lobner, D.; Wheeler, M.; Almli, C. R.; Shen, C. K.-F.; Luh, T.-Y.; Choi, D. W.; Lin. T.-S. *Proc. Natl. Acad. Sci. U.S.A.* **1997**, *94*, 9434−9439.

(17) Kato, H.; Kanazawa, Y.; Okumura, M.; Taninaka, A.; Yokawa, T.; Shinohara, H. *J. Am. Chem. Soc.* **2003**, *125*, 4391−4397.

(18) Noon, W. H.; Kong, Y.; Ma, J.; *Proc. Natl. Acad. Sci. U.S.A.* **2002**, *99*, 6466−6470.

(19) Zhao, X.; Striolo, A.; Cummings, P. *Biophys. J.* **2005**, *89*, 3856−3862.
(20) Andrievsky, G.; Klochkov, V.; Derevyanchenko, L. *Fullerenes, Nanotubes Carbon Nanostruct.* **2005**, *13*, 363−376.
(21) Colvin, V. L. *Nat. Biotechnol.* **2003**, *21*, 1166−1170.
(22) Sayes, C. M.; Fortner, J D.; Guo, W.; Lyon, D.; Boyd, A. M.; Ausman, K. D.; Tao, Y. J.; Sitharaman, B.; Wilson, L. J.; Hughes, J. B.; West, J. L.; Colvin, V. L. *Nano Lett.* **2004**, *4*, 1881−1887.
(23) Jia, G.; Wang, H.; Yan, L.; Wang, X.; Pei, R.; Yan, T.; Zhao, Y.; Guo, X. *Environ. Sci. Technol.* **2005**, *39*, 1378−1383.
(24) Sayes, C. M.; Gobin, A. M.; Ausman, K. D.; Mendez, J.; West, J. L.; Colvin, V. L. *Biomaterials* **2005**, *26*, 7587−7595.
(25) Li, L.; Bedrov, D.; Smith, G. D. *Phys. Rev. E* **2005**, *71*, 011502−1−4.
(26) Li, L.; Bedrov, D.; Smith, G. D. *J. Phys. Chem. B* **2006**, *110*, 10509−10513.
(27) Li, L.; Bedrov, D.; Smith, G. D. *J. Chem. Phys.* **2005**, *123*, 204504-(1−7).
(28) Bassolino-Klimas, D.; Alper, H. E.; Stouch, T. R. *J. Am. Chem. Soc.* **1995**, *117*, 4118−4129.
(29) Bassolino-Klimas, D.; Alper, H. E.; Stouch, T. R. *Biochemistry* **1993**, *32*, 12624−12637.
(30) Grossfield, A.; Woolf, T. B. *Langmuir* **2002**, *18*, 198−210.
(31) Xiang, T. *J. Phys. Chem. B* **1999**, *103*, 385−394.
(32) Sugii, T.; Takagi, S.; Matsumoto, Y. *Thermal Sci. Eng.* **2004**, *12*, 1−2.
(33) Berendsen, H. J. C.; Marrink, S. J. *Pure Appl. Chem.* **1993**, *65*, 2513−2520.
(34) Marrink, S. j.; Berendsen, H. J. C. *J. Phys. Chem.* **1994**, *98*, 4155−4169.
(35) Zahn, D.; Brickmann, J. *Phys. Chem. Chem. Phys.* **2001**, *3*, 848−852.
(36) Jedlovszky, P.; Mezei, M. *J. Am. Chem. Soc.* **2000**, *122*, 5125−5131.
(37) Jedlovszky, P.; Mezei, M. *J. Phys. Chem. B* **2003**, *107*, 5322−5332.
(38) Bemporad, D.; Essex, J. W.; Luttmann, C. *J. Phys. Chem. B* **2004**, *108*, 4875−4884.
(39) Lopez, C. F.; Nielson, S. O.; Ensing, B.; Moore, P. B.; Klein, M. *Biophys. J.* **2005**, *88*, 3083−3094.
(40) Feller, S. E.; Brown, C. A.; Nizza, D. T.; Gawrisch, K. *Biophys. J.* **2002**, *82*, 1396−1404.
(41) Sum, A. K.; de Pablo, J. J. *Biophys. J.* **2003**, *85*, 3636−3645.
(42) Ulander, J.; Haymet, A. D. J. *Biophys. J.* **2003**, *85*, 3475−3484.
(43) MacCallum, J. L.; Tieleman, D. P. *J. Am. Chem. Soc.* **2006**, *128*, 125−130.
(44) Marrink, S. J.; Berendsen, H. J. C. *J. Phys. Chem.* **1996**, *100*, 16729−16738.
(45) Chang, R.; Violi, A. *J. Phys. Chem. B* **2006**, *110*, 5073−5083.
(46) Srinivas, G.; Klein, M. L. *Nanotechnology* **2004**, *15*, 1289−1295.
(47) Tasseff, R. A.; Kopelevich, D. I. *J. Undegr. Res.* **2006**, *7*(4).
(48) Qiao, R.; Roberts, A. P.; Mount, A. S.; Klaine, S. J.; Ke, P. C.; *Nano Lett.* **2007**, *7*, 614−619.
(49) Foloppe, N.; MacKerell, A. D., Jr. *J. Comput. Chem.* **2000**, *21*, 86−104.
(50) Jorgensen, W. L.; Chandrasekhar, J.; Madura, J. D.; Impey, R. W.; Klein, M. L. *J. Chem. Phys.* **1983**, *79*, 926−935.
(51) Girifalco, L. A. *J. Phys. Chem.* **1992**, *96*, 858−862.
(52) Bedrov, D.; Smith, G. D.; Li, L. *Langmuir* **2005**, *21*, 5251−5255.
(53) Nosé, S. *J. Chem. Phys.* **1984**, *81*, 511−519.
(54) Hoover, W. G. *Phys. Rev. A* **1985**, *31*, 1695−1697.
(55) Anderson, H. C. *J. Chem. Phys.* **1980**, *72*, 2384−2393.
(56) Ryckaert, J.; Ciccotti, G.; Berendsen, H. J. C. *J. Comput. Phys.* **1977**, *23*, 327−341.
(57) Allen M. P.; Tildesley, D. J. *Computer Simulations of Liquids*; Oxford: New York, 1987.
(58) Darden, T.; York, D.; Pedersen, L. *J. Chem. Phys.* **1993**, *98*, 10089−10092.
(59) Martyna, G. J.; Tuckerman, M. E.; Tobias, D. J.; Klein, M. L. *Mol. Phys.* **1996**, *87*, 1117−1157.
(60) Janiak, M. J.; Small, D. M.; Shipley, G. G. *Biochemistry* **1976**, *15*, 4575−4580.
(61) Li, L.; Devande, H.; Bedrov, D.; Smith, G. D. *J. Phys. Chem. B* **2007**, *111*, 4067−4072.
(62) Yoshihara, T.; Murai, M.; Tamaki, Y.; Furube, A.; Katoh, R. *Chem. Phys. Lett.* **2004**, *394*, 161−164.
(63) Sivaraman, N.; Dhamodaran, R.; Kaliappan, I.; Srinivasan, T. G.; Vasudeva, P. R.; Mathews, C. K. *J. Org. Chem.* **1992**, *57*, 6077−6079.
(64) Ruoff, R. S.; Tse, D. S.; Malhotra, R.; Lorents, D. *J. Phys. Chem.* **1993**, *97*, 3379−3383.
(65) Stukalin, E. B.; Korobov, M. V.; Avramenko, N. V. *J. Phys. Chem. B* **2003**, *107*, 9692−9700.
(66) Bemporad, D.; Luttmann, C.; Essex, J. W. *Biophys. J.* **2004**, *87*, 1−13.